

Original article

Understanding the antitumor activity of novel tricyclicpiperazinyl derivatives as farnesyltransferase inhibitors using CoMFA and CoMSIA

D.S. Puntambekar, R. Giridhar, M.R. Yadav*

Pharmacy Department, Faculty of Technology and Engineering, The MS University of Baroda, Vadodara-390001, Gujarat, India

Received in revised form 2 July 2006; accepted 3 July 2006

Available online 21 August 2006

Dedicated to Sharad Puntambekar on his 57th Birthday

Abstract

3D-QSAR studies of some tricyclicpiperazinyl derivatives as farnesyltransferase inhibitors were performed by comparative molecular field analysis (CoMFA) and comparative molecular similarity indices (CoMSIA) methods to rationalize the structural requirements responsible for the inhibitory activity of these compounds. The global minimum energy conformer of the template molecule **35**, the most active and pharmacokinetically stable molecule of the series, was obtained by simulated annealing method and used to build structures of the molecules in the dataset. The CoMFA model obtained after the removal of outliers produced statistically significant results with cross-validated and conventional correlation coefficients of 0.550 and 0.969, respectively. The combination of steric, electrostatic, hydrogen bond acceptor and hydrophobic fields in CoMSIA gave the best results with cross-validated and conventional correlation coefficients of 0.611 and 0.986, respectively. The predictive ability of CoMFA and CoMSIA were determined using a test set of 24 tricyclicpiperazinyl derivatives giving predictive correlation coefficients of 0.543 and 0.663, respectively, indicating good predictive power. Further the robustness of the model was verified by bootstrapping analysis. Based on the CoMFA and CoMSIA analysis we have identified some key features in the tricyclicpiperazinyl series that are responsible for farnesyltransferase inhibitory activity that may be used to design more potent tricyclicpiperazinyl derivatives and predict their activity prior to synthesis.

© 2006 Elsevier Masson SAS. All rights reserved.

Keywords: 3D-QSAR; CoMFA; CoMSIA; Farnesyl protein transferase**1. Introduction**

Mutations in the *ras* oncogene have been detected in a wide variety of human tumors, with the highest incidence being observed in the cancers of pancreas (90%), colon (50%), and lung (30%) [1]. The important role played by Ras protein in the signal transduction process involved in cell division is well recognized [1,2]. Inhibition of farnesylation of the Ras protein, a key step in the posttranslational modification of this protein [3,4] continues to be the subject of intense interest as a source of potential antitumor agents. This has led to the synthesis of several novel groups of farnesyl protein transferase (FPT) inhibitors which have been reviewed [5], most of which are peptidic or peptidomimetic in nature. Most of these are CaaX

mimetics, while others are farnesyl diphosphate analogs, or natural products derived from screening programs.

Random screening of chemical libraries also led to the identification of several nonpeptides, non-thiol compounds, which were optimized into R-115777, SCH-66336 and BMS-214662 which are presently engaged in clinical trials [6]. Various attempts have also been made to increase the membrane permeability of farnesyltransferase inhibitors by preparing ester prodrugs [7]. Recently Li et al. [8] reported achiral analogs of 2-quinolines and indoles as non-thiol farnesyltransferase inhibitors and some benzimidazolones based on tipifarnib scaffold [9]. Santagada et al. [10] reported the synthesis, pharmacological evaluation and molecular modeling studies of novel peptidic CAAX analogs as potential farnesyltransferase inhibitors. Protein farnesyltransferase inhibitors have also been recently reported to exhibit potent antimalarial activity [11]. Recently Lane and Beese [12] have explored the structural biology of protein farnesyltransferase and geranylgeranyltransferase type I, while Eastman et al.

* Corresponding author.

E-mail addresses: mryadav@sify.com, devendra_res@yahoo.co.uk (M.R. Yadav).

[13] have discussed the importance of blocking protein farnesyltransferase in fighting against parasitic diseases.

The ligand based approaches like 3D-QSAR studies are quite useful to rationalize the structural requirements required for enzyme inhibitory activity. Similar approach was also used by us in rationalizing the structural requirements for COX-2 inhibitory activity [14] and also in identifying the structural requirements in the series of benzonitrile derivatives using comparative molecular field analysis (CoMFA) [15]. We report herein the results of CoMFA and comparative molecular similarity indices (CoMSIA) performed on a series of tricyclic piperazinyl derivatives as farnesyltransferase inhibitors (Tables 1 and 2). The 3D-QSAR analyses can provide more insight into the optimization of this series of farnesyltransferase inhibitors. Since its introduction in 1988, CoMFA [16] has rapidly evolved to be one of the most powerful tool for 3D-QSAR studies [17,18]. CoMFA methodology is based on the assumption that the changes in the biological activity correlate with the changes in the steric and electrostatic fields of the molecules. The CoMSIA method [19] differs by the way the molecular fields are calculated and by including additional molecular fields such as lipophilic and hydrogen bond potential. The additional fields in CoMSIA provide better visualization and interpretation of the obtained correlation in terms of field contribution to the activity of the compound. On the basis of CoMFA and CoMSIA models developed for tricyclic piperazinyl derivatives, we attempted to elucidate a structure–activity relationship to provide useful information for the designing of new farnesyltransferase inhibitors with enhanced biological activity prior to synthesis.

2. Results and discussion

2.1. CoMFA and CoMSIA analyses

The results of CoMFA and CoMSIA studies are summarized in Tables 3 and 4, respectively. All the analyses reveal comparable cross-validated r^2 values. Analysis-A (Table 3) yielded a correlation with an r^2_{cv} of 0.399 (eight principal components) and a conventional r^2 of 0.823. This model displayed poor external predictivity with r^2_{pred} 0.275. Thus, in order to increase the predictive power of the derived model, further experiments were performed. Based on the results of QSAR studies from partial least square (PLS) analysis nine molecules (compounds 7, 15, 17, 23, 38, 44, 45, 60 and 111) of the training set with high residual values were omitted. Analysis-B (Table 3) shows the CoMFA results obtained using the training set of 93 compounds showed better confidence level in statistical significance. Analysis-B showed improved cross-validated r^2 of 0.550, conventional r^2 of 0.969, F value of 121.990, bootstrapped r^2 of 0.947 and predictive r^2 of 0.543. The steric and electrostatic contributions were found to be 46.2% and 53.8%, respectively. The higher contribution of electrostatic fields indicates that the electrostatic interactions of the molecule with the receptor could be an important factor for antitumor activity.

CoMSIA analysis was performed using steric, electrostatic, hydrophobic and hydrogen bond donor and hydrogen bond acceptor fields. Presently CoMSIA offers five different fields;

3D-QSAR models can be generated using the above fields in different combinations. The results of CoMSIA analysis are summarized in Table 4. The CoMSIA models showed considerable correlative and predictive properties. In most of the models, hydrophobic field was a common factor indicating the importance of lipophilicity for the present series of molecules. The model generated using steric, electrostatic and hydrophobic descriptors has higher r^2_{cv} and comparable r^2_{pred} than rest of the models but has higher standard error of estimate and standard error of prediction. Incorporation of all the fields resulted in the reduction of r^2_{cv} and r^2_{pred} . To check whether the addition of hydrogen bond donor or acceptor descriptors affect the model, each descriptor was considered along with steric, electrostatic and hydrophobic descriptors for generating the model. It was observed that inclusion of hydrogen bond donor descriptor caused reduction in r^2_{cv} (0.580). Where as the addition of hydrogen bond acceptor caused increase in the r^2_{cv} (0.611) and also the predictive power (r^2_{pred}) of the model. This indicates the importance of hydrogen bond acceptor functional group for the biological activity. Finally the combination of steric, electrostatic, hydrophobic and hydrogen bond acceptor was selected as the best model on the basis of presence of proper (a) statistical terms and (b) descriptors to explain observed biological activity.

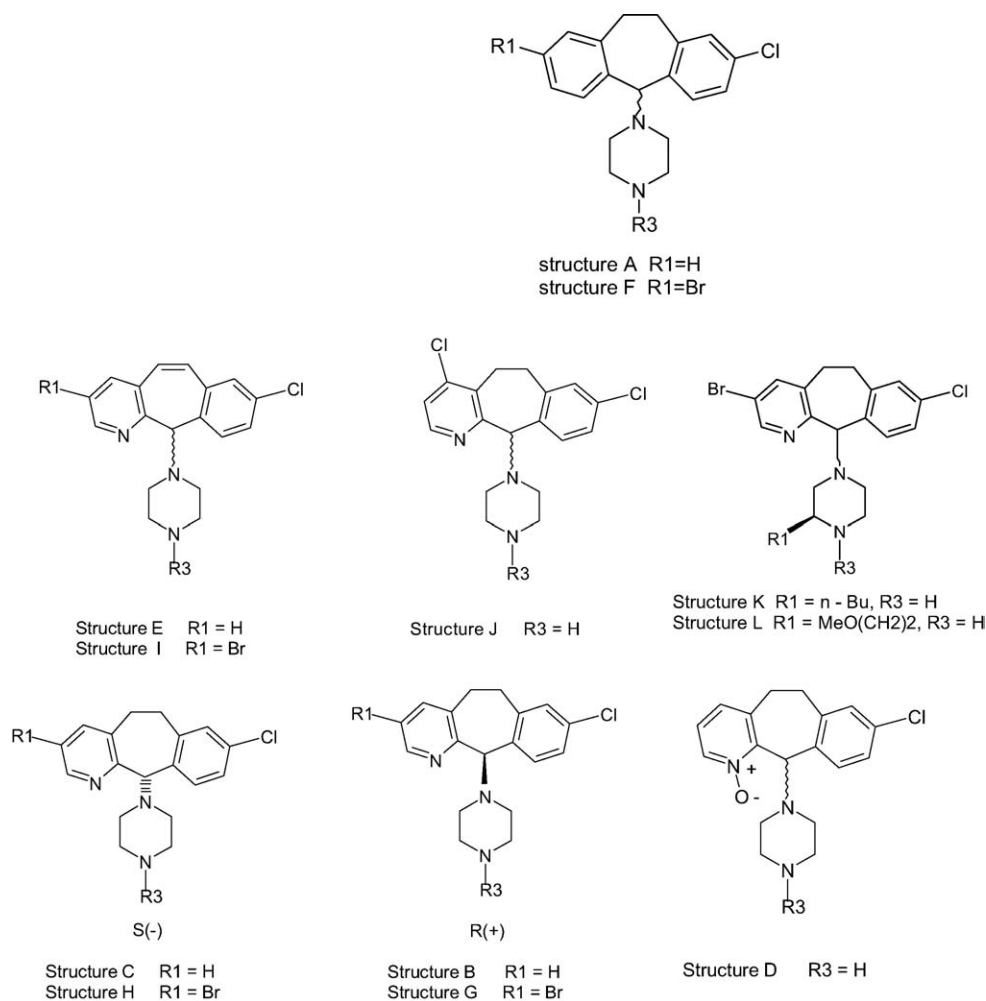
The real test for the model predictiveness is to predict the activity of compounds, which were not used in the model generation. To check the external predictivity of the model, we used the test set, which comprised of 24 compounds. Both the CoMFA and CoMSIA models exhibited a good predictiveness on these compounds. The observed and calculated activity values for training and test set molecules are given in Tables 5 and 6, respectively. The plots of calculated vs. observed activity values for training set molecules and predicted vs. observed activity values for the test set molecules are shown in Figs. 5 and 6, respectively. The actual, predicted and residual values of training and test set for CoMFA and CoMSIA are given in Tables 5 and 6, respectively.

2.2. Graphical interpretation of the results

To visualize the information content of the derived 3D-QSAR model, CoMFA contour maps were generated by interpolating the products between the 3D-QSAR coefficients and their associated standard deviations. Figs. 3 and 3a indicate the CoMFA steric and electrostatic contour maps, respectively, obtained from analysis-B using compound 35 as a reference structure. In this figure, the green contours represent regions of high steric tolerance (80% contribution), while the yellow contours represent regions of low steric bulk tolerance (20% contribution). The increase in positive charge is favored in blue regions while increase in negative charge is favored in red regions.

The steric contour of CoMFA (Fig. 3) shows a large green contour enclosing the pyridyl acetyl N-oxide (R_3 substituent) of the template structure. This indicates that bulky R_3 substituents on the piperazine will enhance the farnesyltransferase inhibitory activity. The good inhibitory potency of 70 (IC₅₀ 0.049),

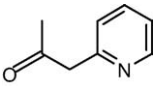
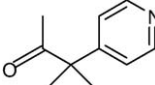
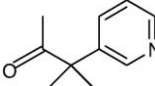
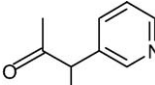
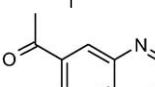
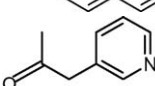
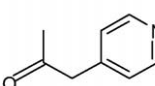
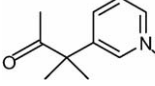
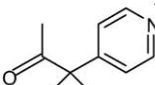
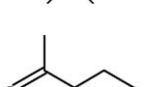
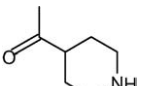
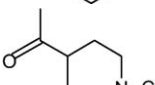
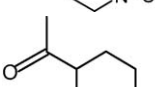
Table 1
Structures and antitumor activity of compounds used in training set



Compound number	Structure	R ₃	IC ₅₀ (μM)	pIC ₅₀ (μM)
1	A	-H	30.3	4.51
2	A		0.82	6.08
3	A	-COCH ₂ NHBoc	4.8	5.31
4	A	-COCH ₂ NHCOCH(SH)CH ₃	2.78	5.55
5	A	-COCH(C ₆ H ₅) ₂	2.5	5.60
7	A	-COCH ₂ C ₆ H ₄ -4-Br	2.04	5.61
8	A	-COCH ₂ C ₆ H ₄ -4-NMe ₂	2.44	4.69
9	A	-COC ₆ H ₄ -4-NMe ₂	20.2	6.79
10	A		0.16	7.92
11	F		0.012	6.85
12	C		0.14	6.27
13	A		0.53	6.76
14	F		0.17	6.04
15	C		0.19	6.05
16	D		0.91	6.44
17	E		2.1	5.75

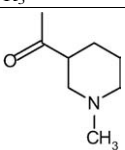
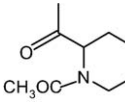
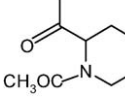
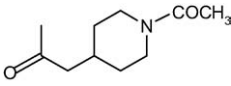
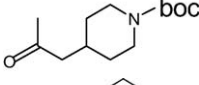
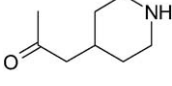
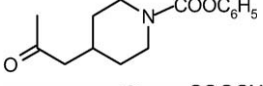
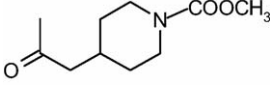
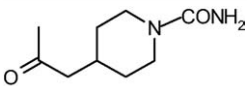
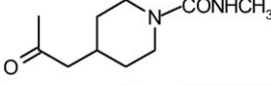
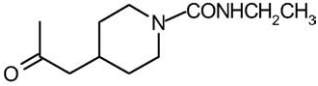
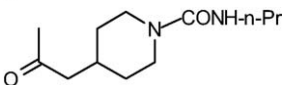
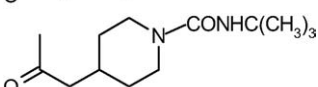
(continued)

Table 1 (continued)

Compound number	Structure	R ₃	IC ₅₀ (μM)	pIC ₅₀ (μM)
18	J		0.88	6.07
19	A		0.36	5.30
21	A		1.74	5.74
22	A		0.85	5.93
23	F		0.3	6.39
24	A		4.9	5.42
26	F		1.8	5.34
27	A		1.17	6.13
28	F		0.4	7.32
30	D		3.8	6.30
31	E		4.5	6.48
32	A		0.74	5.90
33	F		0.047	5.65
34	C		0.49	6.40
36	J		0.33	5.90
38	L		0.034	4.87
39	A		1.26	5.36
41	A		2.2	5.16
42	F		0.39	4.99
43	A		1.24	5.85
44	C		1.8	6.19
45	A		11.3	5.86
46	A		13.3	6.34
47	A		4.3	6.06

(continued)

Table 1 (continued)

Compound number	Structure	R ₃	IC ₅₀ (μM)	pIC ₅₀ (μM)
48	A		6.8	5.79
49	A		10.2	5.13
50	A		1.4	5.90
52	C		0.64	7.14
54	E		1.37	7.10
55	J		0.45	7.08
56	A		0.87	7.16
58	C		1.6	6.46
59	A		7.4	5.88
60	F		1.29	6.08
61	A		1.25	7.31
62	F		0.072	7.31
63	G		0.078	7.34
64	I		0.083	7.56
65	L		0.069	7.03
66	F		0.34	5.97
67	A		1.3	6.03
69	A		0.82	6.05
70	F		0.049	6.00
71	H		0.048	6.96
72	I		0.045	5.60
73	K		0.027	5.60
74	L		0.092	5.95
75	A		1.05	6.98
77	A		0.92	6.63
78	A		0.88	5.92
80	A		1.0	7.00
81	F		0.108	6.22

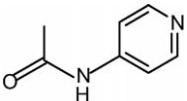
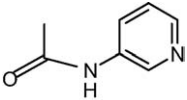
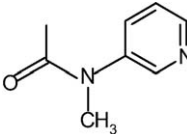
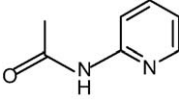
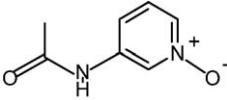
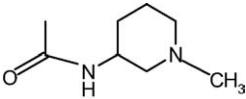
(continued)

Table 1 (continued)

Compound number	Structure	R ₃	IC ₅₀ (μM)	pIC ₅₀ (μM)
83	A		2.5	5.77
84	A		2.5	5.15
85	A		1.1	5.15
86	F		0.104	5.85
88	F		0.23	6.30
89	A		1.19	6.08
90	F		0.1	5.50
91	C		0.6	6.50
92	E		1.66	5.67
96	A		7.0	6.05
98	A		7.0	5.00
99	F		1.4	5.75
101	A		0.5	5.96
102	C		0.82	6.04
103	A		3.1	5.87
105	F		0.31	6.67
106	A		2.1	6.33
108	E		0.88	5.33
109	A		9.8	6.02
110	F		1.77	6.67
111	A		4.1	5.65
112	A		1.09	6.61

(continued)

Table 1 (continued)

Compound number	Structure	R ₃	IC ₅₀ (μM)	pIC ₅₀ (μM)
113	A		0.9	7.38
114	A		1.34	6.18
115	F		0.21	7.26
116	C		0.46	6.33
117	A		4.6	5.33
118	A		0.95	6.02
120	F		0.21	6.67
121	A		2.2	5.65
122	F		0.24	6.61
124	F		0.041	7.38
125	A		0.66	6.18
126	F		0.054	7.26

71 (IC₅₀ 0.048), **72** (IC₅₀ 0.045), **73** (IC₅₀ 0.027) and **74** (IC₅₀ 0.092) are due to orientation of their 4-carboxamidopiperidinylacetamido group towards sterically favored green contour. Compound **1** lacking bulky group at the fourth position of the piperazine was inactive. The steric contours also show yellow contour in the vicinity of the aromatic ring of the R₃ substituent attached to the piperazine. Here bulky substituents are not tolerated and hence the molecules **4** (IC₅₀ 2.78), **66** (IC₅₀ 0.34) and **110** (IC₅₀ 1.77) exhibit low inhibitory activity.

The electrostatic contours of CoMFA (Fig. 3a) shows red contour enclosing the pyridine ring of the template molecule where high electron density is expected to increase the activity. Hence the N-oxide derivatives (**33**, **34**, **36**, **38**, **124**) exhibit good activity where the electronegative oxygen is buried in red contour. This is because N-oxide increases electron density which is favorable for inhibitory activity. The electrostatic contours also show blue polyhedra in the vicinity of piperazine ring where low electron density is expected to increase activity. Compound **7** (IC₅₀ 2.04) exhibits low activity as the electronegative bromide group is embedded in the blue contours.

The hydrophobic contours (Fig. 4) show presence of a large purple contour surrounding the pyridine ring of the template molecule indicating that hydrophobic substituents are well tolerated in that region. The hydrogen bond acceptor contours (Fig. 4a) show presence of small magenta contours close to the piperazine ring of the template molecule, where hydrogen

bond acceptor substituents will increase the activity. Two cyan contours are seen; one close to the pyridyl nitrogen and one enclosing the aromatic substituent attached to piperazine indicate regions in space where hydrogen bond acceptor groups are not tolerated. The developed CoMFA and CoMSIA models are predictive enough to guide the design of new molecules.

2.3. CoMFA vs. CoMSIA

The comparison of the statistical results of two QSAR analyses is listed in Table 7. The cross-validated r^2 , conventional correlation coefficient r^2 , and predictive r^2 are normally accepted as the statistical measures for the quality of QSAR models. Both CoMFA and CoMSIA models exceeded $r^2_{cv} > 0.5$ which indicated stability of the model and reasonable predictability [20]. CoMSIA showed higher cross-validated r^2 value of 0.611 than 0.550 for CoMFA. The standard error of estimate was also less (0.123) than CoMFA (0.215). Finally the predictive power (r^2_{pred}) value was also on a higher side for CoMSIA than CoMFA.

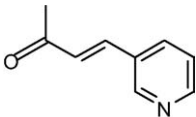
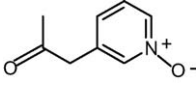
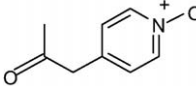
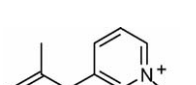
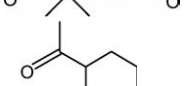
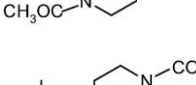
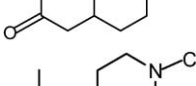
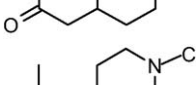
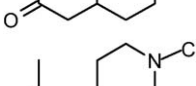
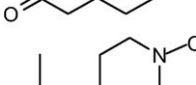
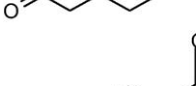
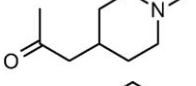
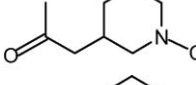
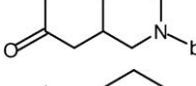
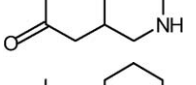
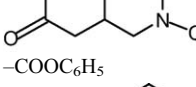
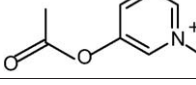

3. Experimental

3.1. Dataset for analysis

One hundred and twenty-six molecules selected for the present study were taken from the published work by Mallam et

Table 2

Structures and antitumor activity of compounds used in test set

Compound number	Structure	R ₃	IC ₅₀ (μM)	pIC ₅₀ (μM)
6	A	–COCH ₂ C ₆ H ₅	2.73	5.56
20	A	–COC(CH ₃) ₂ C ₆ H ₅	3.3	5.48
25	A		2.6	5.58
29	C		2.3	5.63
35	H		0.023	7.63
37	K		0.06	6.22
40	F		0.38	6.42
51	F		0.12	6.92
53	H		0.05	7.30
57	F		0.102	7.00
68	A		1.27	5.89
76	F		0.05	7.30
79	F		0.1	7.00
82	A		0.88	6.05
87	A		1.89	5.72
93	A		3.1	5.50
94	A		12.2	4.91
95	A		1.1	5.95
97	A		1.75	5.75
100	A	–COOC ₆ H ₅	0.8	6.09
104	F		0.28	6.55

(continued)

Table 2 (continued)

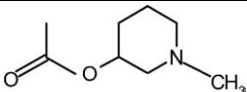
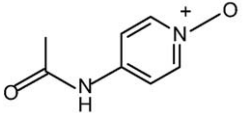
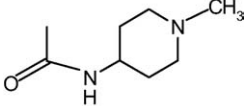
Compound number	Structure	R ₃	IC ₅₀ (μM)	pIC ₅₀ (μM)
107	F		0.3	6.52
119	A		1.8	5.74
123	A		0.47	6.32

Table 3
Summary of CoMFA analysis

Parameter	CoMFA (analysis-A)	CoMFA (analysis-B)
r^2_{cv}	0.399	0.550
SEP	0.350	0.480
N	8	6
r^2	0.823	0.909
SEE	0.340	0.215
F value	83.045	121.990
Prob. of $r^2 = 0$	0.0	0.0
r^2_{pred}	0.375	0.543
r^2_{bs}	0.880	0.947
S.D.	0.087	0.011
Contributions (%)		
Steric	0.450	0.462
Electrostatic	0.550	0.538

al. [21]. It is imperative to evaluate the predictivity of the 3D-QSAR models generated. Selection of the training set and test set molecules was done by considering the fact that test set molecules represent a range of biological activity similar to that of the training set. Thus, the test set is the true representative of the training set. The structures of the training and test

Table 4
Summary of CoMSIA analysis

	r^2_{cv}	SEP	N	r^2	SEE	F	r^2_{bs}	SD	r^2_{pred}
H ^a	0.475	0.503	2	0.925	0.199	96.355	0.961	0.009	0.383
D ^b	0.140	0.653	4	0.619	0.447	14.395	0.676	0.057	0.108
A ^c	-0.161	0.744	1	0.629	0.441	15.043	0.754	0.058	-0.202
D + A	-0.039	0.717	4	0.798	0.323	40.457	0.868	0.023	0.123
H + D	0.574	0.459	4	0.900	0.227	92.315	0.936	0.016	0.282
H + A	0.454	0.520	4	0.934	0.185	145.364	0.962	0.010	0.667
H + D + A	0.508	0.493	4	0.939	0.177	158.138	0.965	0.008	0.541
H + S ^d + E ^e	0.631	0.430	6	0.953	0.156	208.365	0.973	0.005	0.529
S + E + D	0.451	0.520	6	0.957	0.149	230.015	0.970	0.006	-0.007
S + E + A	0.355	0.577	7	0.944	0.169	174.930	0.960	0.012	0.544
S + E + D + A	0.399	0.557	7	0.958	0.148	233.327	0.965	0.005	0.554
S + E + D + A + H	0.535	0.493	8	0.980	0.101	445.103	0.987	0.001	0.634
S + E + A + H ^f	0.611	0.451	6	0.971	0.123	299.318	0.986	0.004	0.663
S + E + D + H	0.580	0.469	8	0.980	0.101	445.103	0.991	0.006	0.621
ALL	0.466	0.514	4	0.976	0.113	354.709	0.984	0.005	0.401

^a Hydrophobic field.

^b Hydrogen bond donor field.

^c Hydrogen bond acceptor field.

^d Steric field.

^e Electrostatic field.

^f Best model for CoMSIA.

set molecules are given in Tables 1 and 2, respectively. The biological activity used in the present study was expressed as

$$pIC_{50} = -\log IC_{50}$$

where IC₅₀ is the concentration (μM) of the inhibitor producing 50% inhibition of protein farnesyltransferase.

3.2. Molecular modeling

All the molecular modeling studies, CoMFA and CoMSIA reported herein were performed on a Silicon Graphics O₂ workstation using SYBYL 6.9 molecular modeling software from Tripos, Inc., St. Louis, MO [22]. All the compounds were built from fragments in the SYBYL database. Each structure was fully geometry-optimized using the standard Tripos force field [23] with a distance-dependent dielectric function until a root mean square (rms) deviation of 0.001 kcal mol⁻¹ Å⁻¹ was achieved.

The conformational search was performed using MULTI-SEARCH option in SYBYL. The minimum energy conformation thus obtained was minimized using the Tripos force field

Table 5

Actual, predicted inhibitory activities (pIC_{50}) and residuals of the training set molecules (using analysis-B of CoMFA and best model from CoMSIA analysis)

Compound numbers	Actual pIC_{50}	Predicted pIC_{50}		Residuals	
		CoMFA	CoMSIA	CoMFA	CoMSIA
1	4.51	4.42	4.50	0.09	0.01
2	6.08	6.32	5.70	-0.24	0.38
3	5.31	5.25	5.52	0.06	-0.21
4	5.55	5.603	5.605	-0.05	-0.07
5	5.60	5.52	5.44	0.08	0.16
8	5.61	5.66	5.64	-0.05	-0.03
9	4.69	4.69	5.01	0.00	-0.32
10	6.79	6.80	6.94	-0.01	-0.14
11	7.92	7.36	7.33	0.56	0.53
12	6.85	6.91	6.55	-0.06	0.30
13	6.27	6.08	6.00	0.19	0.27
14	6.76	6.925	6.927	-0.16	-0.167
16	6.04	6.10	5.97	-0.06	0.07
18	6.05	6.10	6.09	-0.05	-0.04
19	6.44	6.31	6.04	0.11	0.40
21	5.75	5.56	5.75	0.19	0.00
22	6.07	5.53	6.10	0.54	-0.03
24	5.30	5.92	5.21	-0.62	0.09
26	5.74	5.93	5.96	-0.19	-0.22
27	5.93	5.84	5.64	0.09	0.31
28	6.39	6.58	6.60	-0.19	-0.21
30	5.42	5.51	5.49	-0.09	-0.07
31	5.34	5.38	5.40	-0.04	-0.06
32	6.13	6.46	6.28	-0.33	-0.15
33	7.32	7.08	7.20	0.24	0.12
34	6.30	6.21	6.46	0.09	-0.16
36	6.48	6.39	6.42	0.09	0.06
39	5.90	5.92	5.98	-0.02	-0.08
41	5.65	5.71	5.51	-0.06	0.14
42	6.40	6.67	6.47	-0.27	-0.07
43	5.90	5.58	5.68	0.32	0.22
46	4.87	5.00	4.89	-0.13	-0.02
47	5.36	5.20	5.24	0.16	0.12
48	5.16	5.26	5.38	-0.10	-0.22
49	4.99	5.20	5.31	-0.21	-0.32
50	5.85	5.94	5.90	-0.09	-0.05
52	6.19	6.18	6.02	0.01	0.17
54	5.86	5.80	5.82	0.06	0.04
55	6.34	6.25	6.29	0.09	0.05
56	6.06	6.13	5.92	-0.07	-0.86
58	5.79	6.28	6.00	-0.49	-0.21
59	5.13	5.12	5.35	0.01	-0.22
61	5.90	6.00	5.97	-0.10	-0.07
62	7.14	7.11	7.23	0.03	-0.09
63	7.10	6.95	7.34	0.15	-0.24
64	7.08	7.00	7.18	0.08	-0.10
65	7.16	7.38	6.45	-0.22	0.71
66	6.46	6.62	6.54	-0.16	-0.08
67	5.88	5.83	5.66	0.05	0.20
69	6.08	6.24	6.15	-0.16	-0.07
70	7.31	7.21	7.42	0.10	-0.11
71	7.31	6.73	7.18	0.58	0.13
72	7.34	7.11	7.21	0.23	0.13
73	7.56	7.72	7.41	-0.16	0.15
74	7.03	6.98	7.00	0.05	0.03
75	5.97	6.11	5.97	-0.14	0.00
77	6.03	6.09	5.96	-0.06	0.07
78	6.05	6.10	5.96	-0.05	0.09
80	6.00	5.80	5.91	0.20	0.09
81	6.96	6.80	7.03	0.16	-0.07

(continued)

Table 5 (continued)

Compound numbers	Actual pIC_{50}	Predicted pIC_{50}		Residuals	
		CoMFA	CoMSIA	CoMFA	CoMSIA
83	5.60	5.66	5.67	-0.06	-0.07
84	5.60	5.64	5.63	-0.04	-0.03
85	5.95	5.63	5.78	0.32	0.17
86	6.98	6.943	6.94	0.037	0.04
88	6.63	6.82	6.55	-0.19	0.08
89	5.92	5.95	5.94	-0.03	-0.02
90	7.00	6.99	6.78	0.01	0.22
91	6.22	6.20	6.09	0.02	0.13
92	5.77	6.31	6.10	-0.54	-0.33
96	5.15	5.32	5.47	-0.17	-0.32
98	5.15	5.12	4.98	0.03	0.17
99	5.85	6.01	5.77	-0.16	0.08
101	6.30	6.08	5.95	0.22	0.35
102	6.08	6.16	6.13	-0.08	-0.05
103	5.50	5.57	5.63	-0.07	-0.13
105	6.50	6.47	6.46	0.13	0.04
106	5.67	5.18	5.61	0.49	0.06
108	6.05	5.99	6.00	0.06	0.05
109	5.00	4.83	4.73	0.17	0.27
110	5.75	5.78	5.70	0.03	0.05
112	5.96	6.06	5.99	-0.10	-0.03
113	6.04	6.16	6.05	-0.12	-0.01
114	5.87	5.99	6.02	-0.12	-0.15
115	6.67	6.59	6.62	0.08	0.05
116	6.33	6.34	6.39	-0.01	-0.06
117	5.33	5.45	5.49	-0.12	-0.16
118	6.02	5.68	5.82	0.34	0.20
120	6.67	6.53	6.75	0.14	-0.08
121	5.65	5.77	5.78	-0.12	-0.13
122	6.61	6.58	6.68	0.03	-0.07
124	7.38	7.12	7.41	0.26	-0.03
125	6.18	6.18	6.28	0.00	-0.10
126	7.26	7.03	7.15	0.23	0.11

Table 6

Actual, predicted inhibitory activities (pIC_{50}) and residuals of the test set molecules (using analysis – B of CoMFA and best model from CoMSIA analysis)

Compound number	Actual pIC_{50}	Predicted pIC_{50}		Residuals	
		CoMFA	CoMSIA	CoMFA	CoMSIA
6	5.56	5.68	5.60	-0.12	-0.04
20	5.48	5.69	5.97	-0.21	-0.49
25	5.58	5.30	5.81	0.28	-0.23
29	5.63	6.64	6.66	-1.01	-1.03
35	7.63	6.52	6.70	1.11	-0.93
37	6.22	6.54	7.05	-0.32	-0.83
40	6.42	6.80	6.91	-0.38	-0.49
51	6.92	6.90	6.72	0.02	0.20
53	7.30	6.44	6.36	0.86	0.94
57	7.00	7.01	6.86	-0.01	-0.86
68	5.89	5.81	5.84	0.08	0.05
76	7.30	6.98	7.02	0.32	0.28
79	7.00	6.92	7.04	0.08	-0.04
82	6.05	5.60	5.65	0.45	0.40
87	5.72	5.63	5.57	0.09	0.15
93	5.50	6.28	5.94	-0.78	-0.44
94	4.91	5.97	5.74	-1.06	-0.84
95	5.95	6.03	6.06	-0.08	-0.11
97	5.75	5.67	5.80	0.08	-0.05
100	6.09	5.73	5.97	0.36	-0.12
104	6.55	6.22	6.75	0.30	-0.20
107	6.52	6.24	6.48	0.28	0.04
119	5.74	5.41	5.84	0.33	-0.10
123	6.32	6.15	5.97	0.17	0.35

Table 7
Comparison of statistical parameters for two QSAR based models

	r^2_{cv}	SEP	N	r^2	SEE	F	r^2_{bs}	SD	r^2_{pred}
CoMFA	0.550	0.480	6	0.969	0.215	121.990	0.947	0.011	0.543
CoMSIA	0.611	0.451	6	0.971	0.123	299.318	0.986	0.004	0.663

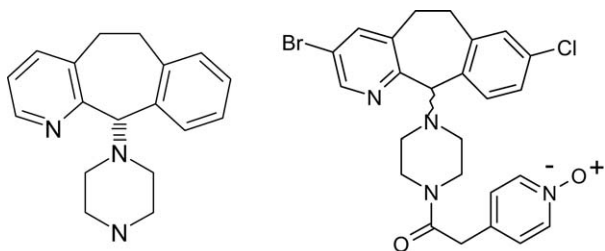


Fig. 1. Common fragment used for alignment and template molecule (compound **35**).

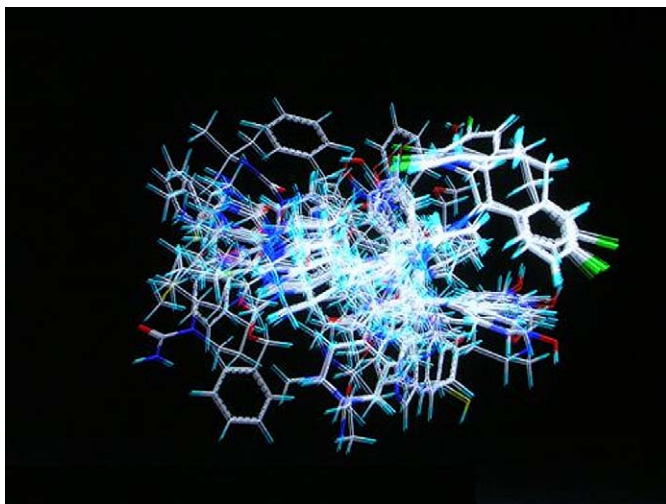


Fig. 2. Alignment of training set of molecules.

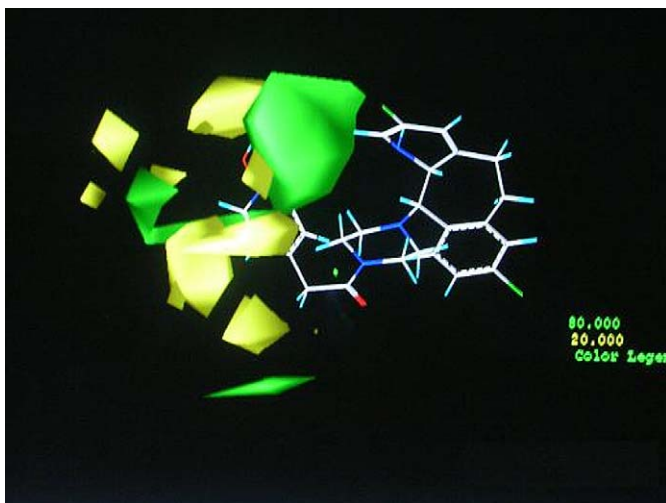


Fig. 3. The CoMFA steric STDEV*COEFF contour plots of active compound **35** from analysis-B. Sterically favored areas (contribution level 80%) are represented by green polyhedra. Sterically disfavored areas (contribution level 20%) are represented by yellow polyhedra.

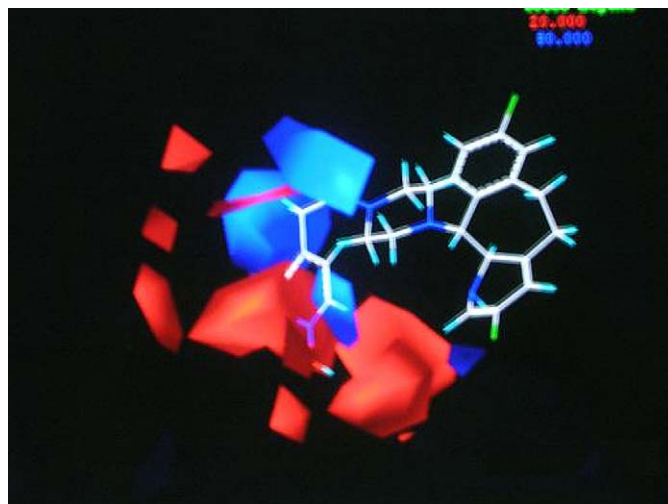


Fig. 3a. The CoMFA electrostatic STDEV*COEFF contour plots of active compound **35** from analysis-B. Positively charged favored areas (contribution level 80%) are represented by blue polyhedra. Negatively charged favored areas (contribution level 20%) are represented by red polyhedra.



Fig. 4. CoMSIA hydrophobic fields. Purple polyhedra indicate regions where hydrophobic substituents are favored and white polyhedra indicate disfavored regions.

and subsequently used in the analyses. Compound **35** the most active compound was chosen as template molecule, on which other molecules were aligned.

3.3. Alignment

One of the most important adjustable parameters in CoMFA is the relative alignment of all the molecules to one another so that they have a comparable conformation and a similar orien-



Fig. 4a. CoMSIA hydrogen bond acceptor contour plots. Magenta polyhedra indicate regions where hydrogen bond acceptor substituents are favored and cyan polyhedra indicates disfavored regions.

tation in space. The most active and pharmacokinetically stable compound **35** was used as a template for superimposition, assuming that its conformation represents the most bioactive conformation of the tricyclicpiperazinyl derivatives at the enzyme active site level. The common fragment shown in Fig. 1 was selected for DATABASE ALIGNMENT method in SYBYL. The aligned compounds are shown in Fig. 2.

3.4. CoMFA interaction energy calculation

The steric and electrostatic fields were calculated at each lattice intersection of a regularly spaced grid of 2.0 Å in all three dimensions within defined region. The vander Waals potential and coulombic term representing the steric and electrostatic fields, respectively, were calculated using standard Tripos force fields. A distance-dependent dielectric constant of 1.00 was used. An sp^3 carbon atom with +1.0 charge was used as a probe atom. The steric and electrostatic fields were truncated at +30.0 kcal mol⁻¹.

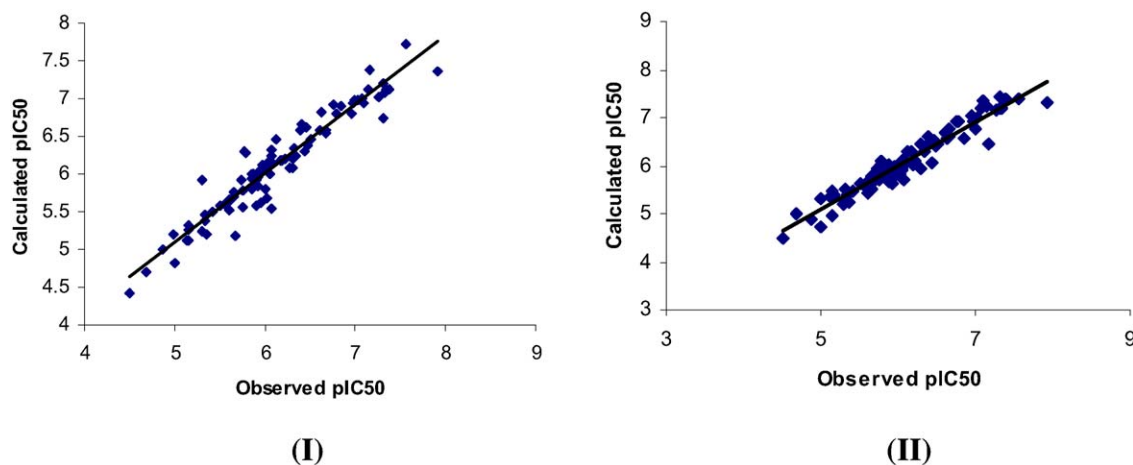


Fig. 5. Calculated vs. observed activity from CoMFA (I) and CoMSIA (II) analyses of the training set.

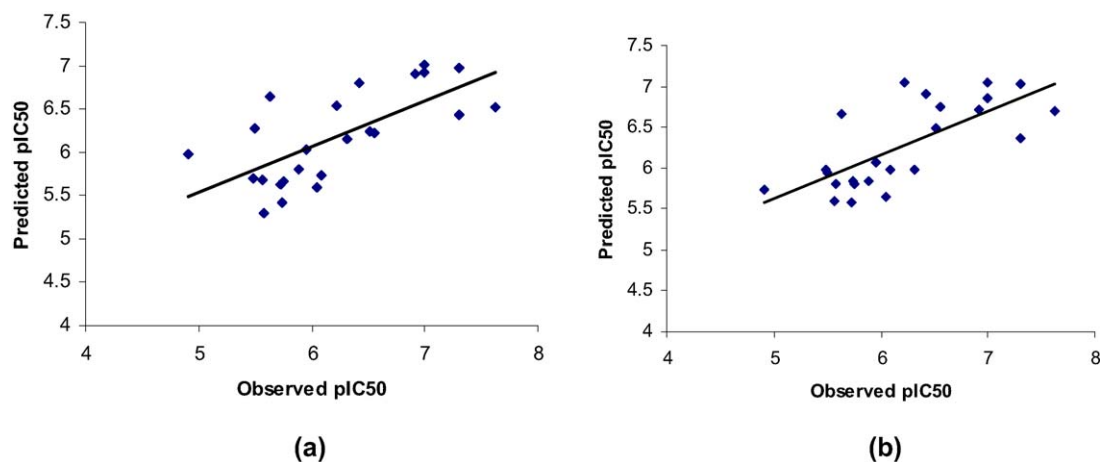


Fig. 6. Predicted vs. observed activity from CoMFA (a) and CoMSIA (b) analyses of the test set.

3.5. CoMSIA interaction energy calculation

The steric, electrostatic, hydrophobic, hydrogen bond donor and hydrogen bond acceptor potential fields were calculated at each lattice intersection of a regularly spaced grid of 2.0 Å. A probe atom with radius 1.0 Å and + 1.0 charge with hydrophobicity of + 1.0 and hydrogen bond donor and hydrogen bond acceptor properties of + 1.0 were used to calculate steric, electrostatic, hydrophobic, donor and acceptor fields. The contribution from these descriptors was truncated at 0.3 kcal mol⁻¹.

3.6. Partial least square (PLS) analysis

PLS method was used to linearly correlate the CoMFA and CoMSIA fields to the inhibitory activity values. The cross-validation [24,25] analysis was performed using the leave one out (LOO) method in which one compound is removed from the data set and its activity is predicted using the model derived from the rest of the dataset. The cross-validated r^2 that resulted in optimum number of components and lowest standard error of prediction were considered for further analysis. Equal weights were assigned to steric and electrostatic fields using COMFA_STD scaling option. To speed up the analysis and reduce noise, a minimum filter value σ of 2.0 kcal mol⁻¹ was used. Final analysis was performed to calculate conventional r^2 using the optimum number of components. To further assess the robustness and statistical confidence of the derived models, bootstrapping analysis for 100 runs was performed. The entire cross-validated results were analyzed by considering the fact that a value of r^2_{cv} above 0.3 indicates that probability of chance correlation is less than 5% [26].

3.7. Predictive correlation coefficient

The predictive ability of each 3D-QSAR model was determined from a set of compounds that were not included in the training set. These molecules were aligned to the template and their activities were predicted. The predictive correlation coefficient (r^2_{pred}), based on molecules of test set, is defined as,

$$r^2_{pred} = (SD - PRESS)/SD$$

where, SD is the sum of the squared deviations between the biological activities of the test set and mean activities of the training molecules and PRESS is the sum of squared deviation between predicted and actual activity values for every molecule in the test set.

4. Conclusions

We have derived a 3D-QSAR model using the CoMFA and CoMSIA method to rationalize the farnesyltransferase inhibitory activity of 126 compounds. The 3D-QSAR equation obtained using the alignment rule showed a high correlative and predictive ability after the removal of outliers. A high bootstrapped r^2 value and small standard deviations indicate

that a similar relationship exists between all compounds. The combination of steric, electrostatic, hydrogen bond acceptor and hydrophobic fields in CoMSIA gave best results. The CoMFA contour maps show a good compatibility with the receptor properties even though the conformations and alignments of ligands were not based on receptor structure. The structural requirements of the inhibitors identified through the CoMFA and CoMSIA contour plots will help in designing new farnesyltransferase inhibitors with enhanced activity.

Acknowledgements

We thank the All India Council for Technical Education (AICTE) [File No. 8021/RID/NPROJ/TAP-201/2002-03] for financial support to develop computer hardware and software facility. One of the authors D.S.P also thank Suresh Kare Indoco foundation for research fellowship.

References

- [1] M. Barbacid, in: C. Richardson (Ed.), *ras Genes*, Annual Reviews Inc., CA, U.S.A, 1997, pp. 779–827.
- [2] A.A. Hall, *Science* 264 (1994) 1413–1414.
- [3] P.J. Casey, P.A. Solski, C.J. Der, J. Buss, *Proc. Natl. Acad. Sci. USA* 86 (1989) 8323–8327.
- [4] K. Kato, A.D. Cox, M.M. Hisaka, S.M. Graham, J.E. Buss, C.J. Der, *Proc. Natl. Acad. Sci. USA* 89 (1992) 6403–6407.
- [5] S.L. Graham, *Exp. Opin. Ther. Pat.* 5 (1995) 1269–1285.
- [6] (a) S.M. Sehti, A.D. Hamilton, *Exp. Opin. Invest. Drugs* 9 (2000) 2767–2782. (b), J.E. Karp, S.H. Kaufmann, A.A. Adjei, J.E. Lancet, J.J. Wright, D.W. End, *Curr. Opin. Oncol.* 13 (2001) 470–476.
- [7] D. Carrico, J. Ohkanda, H. Kdrick, K. Yokoyama, M.A. Blaskovich, C.J. Bucher, F.S. Buckner, W.C.V. Voorhis, D. Chakrabarti, S.L. Croft, M.H. Gelb, S.M. Sehti, A.D. Hamilton, *Bioorg. Med. Chem.* 12 (2004) 6517–6526.
- [8] Q. Li, K.W. Woods, W. Wang, N.H. Lin, A. Claiborne, W. Gu, J. Cohen, V.S. Stoll, C. Hutchins, D. Frost, H.S. Rosenberg, H.L. Sham, *Bioorg. Med. Chem. Lett.* 15 (2005) 2033–2039.
- [9] Q. Li, T. Li, K.W. Woods, W.Z. Gu, J. Cohen, V.S. Stoll, T. Galacia, C. Hutchins, D. Frost, S.H. Rosenberg, H.L. Sham, *Bioorg. Med. Chem. Lett.* 15 (2005) 2918–2922.
- [10] V. Santagada, G. Caliendo, B. Severino, A. Lavecchia, E. Perisutti, F. Fiorino, A. Zampella, V. Sepe, D. Califano, G. Santelli, E. Novellino, *J. Med. Chem.* 49 (2006) 1882–1890.
- [11] L. Nallan, K.D. Bauer, P. Bendale, K. Rivas, K. Yokoyama, C.P. Horney, P.R. Pendyala, D. Floyd, L.J. Lombardo, D.K. Williams, A. Hamilton, S. Sehti, W.T. Windsor, P.C. Weber, F.S. Buckner, D. Chakrabarti, M.H. Gelb, W.C.V. Voorhis, *J. Med. Chem.* 48 (2005) 3704–3713.
- [12] K.T. Lane, L.S. Beese, *J. Lipid Res.* 47 (2006) 681–699.
- [13] R.T. Eastman, F.S. Buckner, K. Yokoyama, M.H. Gelb, W.C. Van Voorhis, *J. Lipid Res.* 47 (2006) 233–240.
- [14] D.S. Puntambekar, R. Giridhar, M.R. Yadav, *Acta Pharm.* 56 (2006) 157–174.
- [15] D.S. Puntambekar, R. Giridhar, M.R. Yadav, *Bioorg. Med. Chem. Lett.* 16 (2006) 1821–1827.
- [16] R.D. Crammer III, D.E. Patterson, J.D. Bunce, *J. Am. Chem. Soc.* 110 (1998) 5959–5967.
- [17] G.R. Desiraju, B. Gopalakrishnan, R.K. Jetty, A. Nagaraju, D. Raveendra, J.A. Sarma, M.E. Sobhia, R. Thilagavathi, *J. Med. Chem.* 45 (2002) 4847–4857.
- [18] G.R. Desiraju, J.A. Sarma, D. Raveendra, B. Gopalakrishnan, R. Thilagavathi, M.E. Sobhia, H.S. Subramanya, *J. Phys. Org. Chem.* 14 (2001) 481–487.

- [19] G. Klebe, U. Abraham, T. Meitzner, *J. Med. Chem.* 37 (1994) 4130–4146.
- [20] S.J. Cho, A. Tropsha, *J. Med. Chem.* 38 (1995) 1060–1066.
- [21] A.K. Mallams, R.R. Rossman, R.J. Doll, V.M. Girijavallabhavan, A.K. Ganguly, J. Petrin, L. Wang, R. Patton, W.R. Bishop, D.M. Carr, P. Kirschmeier, J.J. Catino, M.S. Bryant, K.-J. Chen, W.A. Korfinacher, C. Nardo, S. Wang, A.A. Nomeir, C.C. Lin, Z. Li, J. Chen, S. Lee, J. Dell, P. Lipari, M. Malkowski, B. Yaremkov, I. King, M. Liu, *J. Med. Chem.* 41 (1998) 877–893.
- [22] SYBYL 6.9 is available from Tripos Associates Inc., 1699 S Hanley Rd., St. Louis, MO 63144, USA.
- [23] M. Clark, R.D. Crammer III, V. Opdenbosh, *J. Comput. Chem.* 10 (1989) 982–1012.
- [24] T. Halgren, *J. Am. Chem. Soc.* 112 (1990) 4710–4723.
- [25] B.L. Podlogar, D.M. Fergusson, *Drug Des. Discov.* 17 (2000) 4–12.
- [26] M. Clark, R.D. Crammer III, D.M. Jones, D.E. Patterson, P.E. Simeroth, *Tetrahedron Comput. Methodol.* 3 (1990) 47–59.